Atmospheric Environment 213 (2019) 349–358

Contents lists available at ScienceDirect

Atmospheric Environment

journal homepage: www.elsevier.com/locate/atmosenv

Size-resolved hygroscopicity of ambient submicron particles in a suburban atmosphere

E. Alonso-Blanco*, F.J. Gómez-Moreno, B. Artíñano

Center for Energy, Environmental and Technological Research (CIEMAT), Avenida Complutense 40, 28040 Madrid, Spain

ARTICLE INFO

Keywords:
Aerosol size-resolved hygroscopicity
Mixing state
H-TDMA
Suburban aerosol

ABSTRACT

This work presents a comprehensive study of the size-resolved particle hygroscopicity measurements in a suburban ambient in Southern Europe (Madrid). Measurements were obtained by an H-TDMA instrument during a 16-month period for the size particles of 50, 80, 110, 190 and 265 nm. The annual, seasonal and daily patterns were investigated with the aim of characterizing the hygroscopic growth of ambient aerosol particles and their mixing state in the atmosphere. Simultaneously, the particle number size distributions, gaseous species (SO_2, NO, NO_2, and O_3) and meteorological factors were measured and analyzed, complementing this study. The growth factor probability density functions (GF-PDFs) at the measurement site normally exhibit a multimodal pattern with two hygroscopic groups of particles clearly differentiated, indicating that the aerosol particles were externally mixed. Generally, particle hygroscopicity increased as particles were larger, indicating an increase less-to-more hygroscopic species. In cold seasons, aerosol particles were more externally mixed than in warm seasons. Thus, the growth factor of the more hygroscopic particle group (GF_{MH}) was higher than in warm seasons varying from 1.41 (50 nm)-1.70 (265 nm). However, the number fraction of more hygroscopic particle group (NF_{MH}) was lower. The persistence of anticyclonic stagnation conditions and the enhanced particulate nitrate formation from traffic emissions seemed to be the two main factors responsible for this result. A dominant hygroscopic particle group was often observed in warm seasons, due to frequent NPF bursts. In these seasons, and probably associated to the high atmospheric oxidative capacity, the highest average growth factors (GF_{mean}) of the study period were obtained. This finding was also reflected in the diurnal cycle. Thus, GF_{mean} and NF_{MH} during rush-hour periods usually reached the minimum values of the day, especially in cold seasons. When comparing weekdays and weekends, the strong influence of traffic emissions on particle hygroscopicity was evidenced (WKs/WEs ratios for NF_{MH} were < 1.00). The more dispersive atmospheric conditions in the warm seasons hampered the impact of traffic emissions on particle hygroscopicity. Results from H-TDMA measurements obtained here are similar to those found in other suburban European sites and lower than in suburban Asian ones. With respect to urban sites, our values were lower than those found in urban European and Asian sites. Overall, the findings of this study highlight the strong dependence of the hygroscopic behavior of aerosol particles on the atmospheric conditions and particle sources, and thus, aerosol composition.

1. Introduction

Physical and chemical properties of aerosols determine their behavior and are key factors for their climate and human health effects (Pöschl, 2005). One of the aerosol properties that imply greater uncertainty on the study of those processes and their impacts is the hygroscopicity.

Both the chemical composition of the aerosol particles and the relative humidity (RH) ambient conditions govern the hygroscopic growth of atmospheric aerosols. This may significantly alter a broad range of other aerosol properties, e.g. size distribution, light-scattering and extinction coefficients. Therefore, the liquid water content of the aerosol plays a crucial role in its lifecycle and their effects. For example, this is especially relevant for the indirect effects on climate system (Solomon et al., 2007).

The main way to characterize the hygroscopicity of the aerosol particles is as a function of its dry particle diameter. This can be obtained by employing the tandem differential mobility analyser (TDMA) technique (Liu et al., 1978) through the hygroscopicity tandem DMA or H-TDMA measurements. Unlike other measurement techniques such as nephelometry (Rood et al., 1985) or electrodynamic balance (Davis et al., 1990), the TDMA technique involves a direct measurement of the

* Corresponding author.
E-mail address: elisabeth.alonso@ciemat.es (E. Alonso-Blanco).

https://doi.org/10.1016/j.atmosenv.2019.05.065
Received 16 January 2019; Received in revised form 13 April 2019; Accepted 26 May 2019
Available online 30 May 2019
1352-2310/

aerosol particle size variation with RH providing as well information on the mixing state in terms of hygroscopicity.

Many studies have examined the aerosol particle hygroscopic properties based on ground-based H-TDMA measurements either, on line (Swietlicki et al., 2008) or off-line (Boreddy et al., 2014a, 2014b, 2016) around the world. These studies had different purposes such as characterizing its behaviour with respect to a certain RH (typically 90% RH (Duplissy et al., 2009)) or drawing its metastable equilibrium states though a certain RH gradient (Chen et al., 2003; Cheung et al., 2015). All investigations agreed that the aerosol particle hygroscopicity is strongly dependent on the sources and chemical aging of particles in combination with local characteristics and meteorology.

In 2008, Swietlicki et al. (2008) reviewed previous works and summarized a comprehensive series of studies that collected hygroscopic growth measurements in different environments around the world. The detailed overview highlighted the lack of works in urban environments as well as the short period of hygroscopic growth measurements analyzed in these works. It is well known that in urban areas, one of the largest sources of atmospheric aerosols is fossil fuel combustion that release small carbonaceous particles, mainly formed by black carbon (BC) and organic carbon (OC) (IPCC, 2001), as well as gas-phase species. Once the particles are emitted into the atmosphere, they are quickly modified by a number of physical and chemical processes. Among these processes, the oxidation of gaseous species plays a decisive role in the formation of secondary compounds such as sulfates, nitrates, and a wide range of organic compounds that can be found in a particle phase. These processes determine the growth and coating of aerosols and, therefore, condition their hygroscopicity (Liu et al., 2013).

Although there are currently a higher number of recent works on aerosol particle hygroscopicity measured in urban (Enroth et al., 2018; Kamilli et al., 2014; Kim et al., 2017; Wang et al., 2018) and suburban (Laborde et al., 2013; Müller et al., 2017) sites, there are still important gaps, especially in the suburban case, in the literature related with the geographic distribution of the measurement areas, the scarce number of existing instrumentation and the unavailability of long-term records (see references and information listed in Table S7). In recent years, only results from 7 suburban sites have been found in the literature; three of them on the European continent, three on the Asian continent and one on the American continent. None of suburban European sites is located in the South of Europe, where there is also a special lack of H-TDMA data. These investigations did not analyze more than one year of data, ranging their time series from a few days to several months.

Thus, this work supplements the scarce data of suburban areas in the South of Europe by providing results obtained from H-TDMA measurements at a suburban background site in Madrid. These data cover more than one year (23 September 2014–17 December 2015), the largest H-TDMA database for suburban aerosol found in the literature. The objective of this study is to assess the mixing state and behaviour of the aerosol particles with respect of their hygroscopicity in terms of known sources and meteorology in different temporal scales (seasonal, monthly and daily). For this purpose, additional data on size distribution of aerosol particles, gaseous species and meteorological factors complete this study.

2. Site description and climatology

This study has been carried out in Madrid, Spain, in a measurement station located in the CIEMAT facilities at the north-north western area of the town (40° 27′ 23.2″ N, 03° 43′ 32.3″ E) (Fig. 1).

Madrid is the capital and the most populated city in Spain with ~3 million inhabitants, almost 6 considering the Metropolitan area. This leads to about 2.5 million vehicles circulate daily within the city, of which 1 million corresponds to vehicles enter the city every day. Thus, and in the absence of major industrial activity, road traffic and heating emissions during the cold seasons are the most important contributors to air pollution in Madrid.

The experimental site is surrounded by three green areas (Dehesa de la Villa Park located to the northeast of the CIEMAT, Casa de Campo Park to the southwest and the Monte del Pardo forest area to the northwest). It is not directly affected by any local pollution source. Thus, and due to the diverse surroundings, this site can be considered a representative suburban background site.

The distinctive geography and meteorology of Madrid make it different among many other urban environments. Madrid is surrounded by a mountain range (Sierra de Guadarrama) located about 40 km from the city. This leads to a wind pattern driven by mountain breezes regime, drawing an axis NE-SW parallel to the mountain range. Winds are typically north-easterly at night and during the early morning hours, bringing air from the urban agglomerations (area with traffic emissions) to the site, whereas daytime winds rotate from north-easterly to westerly, bringing air from the Central Mountain System towards the Madrid metropolitan area. Thus, the CIEMAT site shows an aerosol size and composition distribution typical of an urban background site (Gómez-Moreno et al., 2011).

Based on data from the Spanish National Agency for Meteorology (AEMET in its Spanish acronym) the Madrid's climate is considered Continental-Mediterranean, being influenced by urban features.

3. Instrumentation, measurements and methodology

3.1. H-TDMA system: principle of operation and data analysis procedures

The measurements of aerosol particle hygroscopic growth were conducted with a custom-built hygroscopic tandem differential mobility analyser (H-TDMA). This system is based on H-TDMA system developed by Nilsson et al. (2009) following the European Supersites for Atmospheric Aerosol Research (EUSAAR) project recommendations for H-TDMA instruments.

The H-TDMA is formed by two custom-made long Vienna-type Differential Mobility Analyzers (DMAs) in tandem mode linked by a humidification system. Firstly, the polydisperse atmospheric aerosol sample (sample flow of 1 l min^{-1}) is conditioned by a Nafion dryer (RH < 40%) prior to enter the bipolar charger (^{85}Kr). The charged polydisperse aerosol passes through the first DMA (DMA1, R1 = 2.5 cm, R2 = 3.35 cm and L = 28 cm) where a dry discrete particle (D_{dry}) size is selected. Subsequently, the quasi-monodisperse dry particles are conditioned by a humidifying system at a defined RH (in this work a set point of 90%) until the particles reach the equilibrium water uptake. Finally, the aerosol particle size distribution resulting from the humidifier is measured by a second DMA (DMA2, R1 = 2.5 cm, R2 = 3.35 cm and L = 50 cm) connected to a Condensation Particle Counter (CPC-TSI Model 3772), both elements working together as a Scanning Mobility Particle Sizer (SMPS). Both the DMA1 and DMA2 worked with a closed loop system for particle-free sheath air flow (10 and 6 l min^{-1} respectively). All parts of the equipment are conditioned and the H-TDMA system operated between 22 and 23 °C. The instrument configuration allowed the GF measurement of $0.8D_{dry}$-$2.2D_{dry}$, being the minimum and maximum D_{dry} of 50 and 265 nm respectively. Both the instrument regulation and the data acquisition were controlled by a custom LabVIEW software. Further details regarding the H-TDMA system can be found in Alonso-Blanco et al. (2014).

The aerosol particle hygroscopic growth at a RH_{DMA2} of 90% was obtained for mobility diameters of 50, 80, 110, 190 and 265 nm measured at a dry state (RH < 40%). An up and down scan for each dry particle size was made with a resolution of 3 min per scan, i.e., the H-TDMA system can perform a complete scanning each 30 min for the five discrete particle sizes selected. The H-TDMA was checked periodically during the study period for its calibration through the efflorescence behaviour of pure ammonium sulphate for a dry particle size of 110 nm. The H-TDMA was working continuously during the study period except

Fig. 1. (A) Map of Madrid (Spain), (B) the surroundings with the location of the CIEMAT sampling site indicated with a white rectangle and (C) sampling point.

for instrumental failures and calibration tests.

The $TDMA_{inv}$ (Inversion of Tandem Differential Mobility Analyser) method developed by Gysel et al. (2009) was used to invert the H-TDMA data. Dry scans (RH < 10%) of pure ammonium sulphate for the measured sizes were used to calibrate a possible offset between DMA1 and DMA2 and define the width of the H-TDMA's transfer function. The growth factor probability density functions (GF-PDFs) were corrected at 90% RH through κ-model from inversion toolkit to avoid the effect of RH variation, in this study ± 2% from the 90% RH set point. Hygroscopicity scans at higher or lower 90 ± 2% RH_{DMA2} were ignored. A total number of 104,529 H-TDMA data points were obtained from $TDMA_{inv}$ covering the 44.7% of the study period. Measurement coverage varied from 6% (October 2014) to 71% (December 2014). The scan losses were due to an inadequate humidification, measurement artefacts and a low number of accounts for scan due to external atmospheric processes such as dilution/dispersion or wet scavenging. Usually, the larger the particle size, the higher the scan losses were. H-TDMA data coverage by particles size resulted in a 51.8% for 50, 52.1% for 80, 51.9% for 110, 43.7% for 190 and 40.1% for 265 nm (Fig. S1).

From the inversion procedure, GF_{mean} and its spread were obtained. GF_{mean} is defined as the growth factor that would be observed if the absorbed water was equally distributed among all particles of a sample (Sjogren et al., 2008) and expressed by Eq. C.4 in Gysel et al. (2009). Spread (diameter growth spread factor of GF-PDF, σ), is defined as standard deviation of GF-PDF divided by arithmetic mean GF. However, the $TDMA_{inv}$ algorithm has several limitations to characterize in detail the hygroscopicity groups when the GF-PDF is multimodal as it was noted by Sjogren et al. (2008) and subsequently described in detail by Holmgren et al. (2014). Therefore, both Holmgren et al. (2014) and other authors such as Enroth et al. (2018) have proposed, a hygroscopic groups-fitting procedure was development using MATLAB program. Thus, the grown factor (GF), σ and the number fraction (NF) for each hygroscopic group after the data retrieval (Gysel et al., 2009) were obtained. The parameterization was obtained fitting the Gaussian functions to the GF-PDFs. For this purpose, and in order to discriminate between unimodal or bimodal GF-PDFs, the spread of the GF-PDFs of dry particles of ammonium sulphate at 85% RH obtained from $TDMA_{inv}$ have been taken into account according to Sjogren et al. (2008) and Holmgren et al. (2014). The GF-PDF was considered; i) unimodal when the spread was ≤0.10, i.e. the aerosol particles were internally mixed (when all particles of a given size contain the same composition or mixture of different compounds) and ii) bimodal when the spread was > 0.10, i.e. the aerosol particles were externally mixed (when particles of an individual particle size have a mixture of variable relative fractions of different compounds). Note that in this study we only consider those H-TDMA measurements obtained from $TDMA_{inv}$ whose fitting results were significant at 95% confidence interval (t-Student test, $p > 0.05$), a total of 96,562 points distributed in percentage as shown Fig. S1.

In this work, the hygroscopic growth observations were classified into three different types with respect to their mixing state and hygroscopicity based on the parameters obtained from the hygroscopic groups-fitting procedure as suggested by Kim et al. (2017). Given that in GF-PDFs obtained here it was observed a natural cut at GF ~ 1.20 between the less and more hygroscopic particle group, the hygroscopic groups were classified based on this value. When GF-PDF had a bimodal profile, aerosol particles were classified as externally mixed (Type 1), showing two different hygroscopic groups, less-hygroscopic particles (GF < 1.20) and more-hygroscopic particles (GF ≥ 1.20). When GF-PDF presented a unimodal profile and GF ≥ 1.20, aerosol particles were classified as internally mixed and hygroscopic ones (Type 2). Finally, when GF-PDF presented a unimodal profile and GF < 1.20, aerosol particles were classified as internally mixed and hydrophobic ones (Type 3). In this work LH refers to the less-hygroscopic particle group and MH refers to the more-hygroscopic particle one.

GF-PDFs obtained from the $TDMA_{inv}$ frequently exhibited bimodal profiles (type 1). However, some unimodal profiles (types 2 and 3) were also found for all sizes, decreasing their occurrence while size increased (Fig. S2). This has also been observed in other studies such as Gasparini et al. (2004) and Zhang et al. (2011). Monomodal profile accounted for 13.9% of all the measurements, distributed by dry particle size as follows: 6.8% for 50 nm, 3.6% for 80 nm, 2.0% for 110 nm, 0.9% for 190 nm and 0.6% for 265 nm. Exceptionally, a few trimodal profiles of GF-PDF were observed in some days, particularly in March. These last measurements have been considered as bimodal profiles in this work and will be considered for further analysis in a future work.

3.2. Additional instrumentation and complementary measurements

The aerosol particle hygroscopic growth data presented in this work were supplemented by additional data as outlined below.

Particle number size distributions in the range of 15–660 nm were measured by a Scanning Mobility Particle Sizer (TSI-SMPS™: DMA 3081 + CPC 3775) each 4.5 min (Gómez-Moreno et al., 2011). This instrument consists in a Differential Mobility Analyzer (DMA) which allows selecting a known particle size and a Condensation Particle Counter (CPC) system to measure particles number for each size. The corrections by internal diffusion losses of particles in the SMPS and multiple charges were applied to all SMPS scans using the TSI AIM (Aerosol Instrument Manager, TSI Inc.) software. In addition, the diffusional particle losses across of the sample line was estimated as specified the Aerosols, Clouds, and Trace gases Research Infrastructure Network (ACTRIS) standards for SMPS (Wiedensohler et al., 2012) according to Kulkarni et al. (2011), and the aerosol particle size distribution was recalculated.

ACTRIS standard procedures for SMPS maintenance (Wiedensohler et al., 2012) were carried out in order to ensure data quality. Further, the appropriate functioning of the equipment was tested during intercomparison campaigns of the Spanish Network on Environmental DMAs (REDMAAS, in its Spanish acronym) (Gómez-Moreno et al., 2015).

The total particle number concentration (PNC) was obtained from the aerosol particle size distribution. Likewise, the particles concentrations belonging to each of the three modes (nucleation, Aitken and accumulation) were estimated: first particle mode from 15 to 30 nm

(nucleation mode, N_{nuc}), second from 30 to 100 nm (Aitken mode, N_{Ait}), and third from 100 to 660 nm (accumulation mode, N_{acc}).

Standard meteorological parameters were obtained from a meteorological station 52 m high installed near the sampling site. Ambient air temperature at two different heights (Upper and Lower T), relative humidity (RH), wind speed (WS) and wind direction (WD), precipitation (P), atmospheric pressure (AP) and radiation solar (RS) were recorded with a time-resolution of 1 s and averaged to 10-min.

Finally, hourly variability of ambient gases (SO_2, NO, NO_2, and O_3) and particulate matter (PM_{10} and $PM_{2.5}$) concentrations were provided by the suburban air-quality station "Casa de Campo" (3° 44′ 50.44″ W, 40° 25′ 09.68″ N, 645 m a.s.l). This station belongs to the Madrid Municipality air pollution network and is situated about 4.5 km southwest from the sampling site.

All data are provided in Coordinated Universal Time (UTC) and seasons are defined as astronomical seasons.

In tables S1, S2 and S3 a statistics summary of the additional parameters used in this study is shown.

3.3. Derivation of the hygroscopicity parameter κ

Parameter κ captures the combination of the solute properties (Raoult's law (Raoult, 1887)) and the size dependence (Kelvin curvature effect (Thomson, 1872)) of the particles, describing their hygroscopicity. κ-values can be derived directly from the GF data obtained from the $TDMA_{inv}$ algorithm according to *k*-Köhler theory, following the semi-empirical model described in Petters and Kreidenweis (2007) **(1)**:

$$\kappa_{\text{H-TDMA}} = (\text{GF}^3 - 1)\left(\frac{\exp\left(\frac{A}{\text{D}_{\text{dry}}\text{GF}}\right)}{\text{RH}} - 1\right) \quad (1)$$

where GF is the growth factor at 90% RH measured by H-TDMA, *A* is the water activity obtained from Eq. **(2)**, *Ddry* is the dry particle diameter (RH < 40%) and RH is the relative humidity (90%). k-values can range from 0 to 1.

$$A = \frac{4\sigma M_w}{RT\rho_w} \quad (2)$$

where σ is the surface tension (0.0728 N m^{-2}), M_w is the mole weight (18.015 m^3 mol^{-1}), R is the standard gas constant (8.314 J·mol-1·K-1), T is the temperature (297 K) and ρ_w is the density of the solution (1000 kg m^{-3}). The surface tension, mole weight and density of the solution are taken in this work to be those of pure water.

In this study, parameter κ was calculated from our results to facilitate their comparison with other results in the literature. This parameter is widely used in the literature derived experimentally from both, H-TDMA and cloud condensation nuclei counter (CCNc) observations (Petters and Kreidenweis, 2007). Here, given the assumptions made in deriving variability of *k*-values, the empirical growth parametrisation is considered as an analysis tool.

4. Results and discussion

4.1. Overview: meteorology, gases and ultrafine particles

Fig. 2 provides a comprehensive view of the monthly averaged daily evolution of the meteorological conditions over the whole observation period (from 23 September 2014 to 17 December 2015).

Temperature varied between −3.4 and 22.1ºC in the cold seasons vs 1.9 and 38.7 °C in the warm seasons (Table S1), the first associated with the entrance of cold fronts due to strong low pressure centres developed over the North Atlantic. Stagnation episodes associated to atmospheric high-pressure systems over the Iberian Peninsula are more frequent at the end of autumn and during winter (Crespí et al., 1995), causing high concentrations of particles and gases related to traffic and heating emissions (Artíñano et al., 2003; Gómez-Moreno et al., 2011). Thus, between October 2014 and March 2015 and in November and December 2015 hourly PNC exceeded 40,000 cm^{-3} coinciding with high concentrations of NO (up to 247 μg m^{-3}) and NO_2 (up to 133 μg m^{-3}). In addition, the presence of intense surface thermal inversions, as shown by the marked difference between the lower and higher temperature (Fig. 2), as well as the low wind speed registered during these seasons (see WD in Fig. 2), inhibited dispersion of pollutants. Conversely, a higher dispersive capacity of the low atmosphere during the warm seasons, together with a more prominent mountain breeze circulation, promoted the dispersion and dilution of pollutants. Thus, clean periods were frequently observed throughout the warm seasons. Furthermore, the high photochemical activity (high solar radiation intensity and O_3 production) and availability of aerosol forming precursors during these seasons led to new particle formation (NPF) bursts (Alonso-Blanco et al., 2017b, 2018). This implied a considerable contribution of the NPF bursts to the ultrafine particles (UFP) in the area. PNCs were lower in the warm seasons than in the cold ones, in the same way as NO and NO_2. The lowest concentration averages were observed between June and August, with concentrations around 20,000 cm^{-3}, 2–3 μg m^{-3} and 13–16 μg m^{-3} for UFP, NO and NO_2 respectively. Saharan dust episodes are typical of the summer period because of the displacement of warm and dust laden air masses from the North of Africa over the Iberian Peninsula. However, these have a low contribution to UFP and gases but a high contribution to their accumulation. Atlantic fronts passing over the Iberian Peninsula during autumn and spring seasons resulted frequently in heavy rainfall, accumulating the 66% of the total rainfall registered during the whole period of observations. Thus, these situations promoted the diffusion and clearance of pollutants at the site in both seasons. Noteworthy is the low rainfall record of autumn 2015 almost three times smaller than for autumn 2014 (Table S1) and almost two times smaller than normal climatological values of precipitation provided by the AEMET. This led to a higher frequency of stagnation episodes, and caused that daily concentrations for NO (29.1 ± 15.3 μg m^{-3}), NO_2 (37.3 ± 12.9 μg m^{-3}) and UFP (13,422 ± 6410 cm^{-3}) in autumn 2015 were higher than in autumn 2014 (19.6 ± 8.3 μg m^{-3}, 34.4 ± 10.1 μg m^{-3} and 11,596 ± 5108 cm^{-3} respectively) (Fig. S3 and Table S2 and S3). This is in accordance with BC results for the same period at this site (Becerril-Valle et al., 2017).

4.2. Annual variation of hygroscopic properties: seasonal and monthly variation

Hygroscopic properties showed a pronounced variability in time and with particle sizes during the study period (Fig. 3).

Seasonal variations are attributed to meteorological conditions as well as anthropogenic features in this region. Thus, both the shape and the average of the GF-PDFs were substantially variable in time and in particle size. The biggest differences were found between winter and summer. Two groups of particles with different hygroscopic growth were observed in all sizes, implying an aerosol external mixture, except for 50 and 80 nm in the warm seasons (Fig. S4). Particles of these sizes in spring and summer are mainly originated from atmospheric nucleation at the site, probably from biogenic organics compounds (Alonso-Blanco et al., 2017a; Becerril-Valle, 2018). Thus, particles presented an internal mixture (Fig. S2).

Consequently, GF_{mean} also varied greatly with seasons. The greater values were found, on average, in warm seasons caused by a higher oxidative capacity of the atmosphere in Madrid during these seasons (Saiz-Lopez et al., 2017). Some studies have shown that the photochemical oxidation of secondary organic aerosol (SOA) leads to an important increase in its hygroscopicity (Jimenez et al., 2009; Tritscher et al., 2011). Unlike the rest of the sizes measured, the 50 nm particles reached their maximum GF_{mean} values in summer, ~1.22 on average,

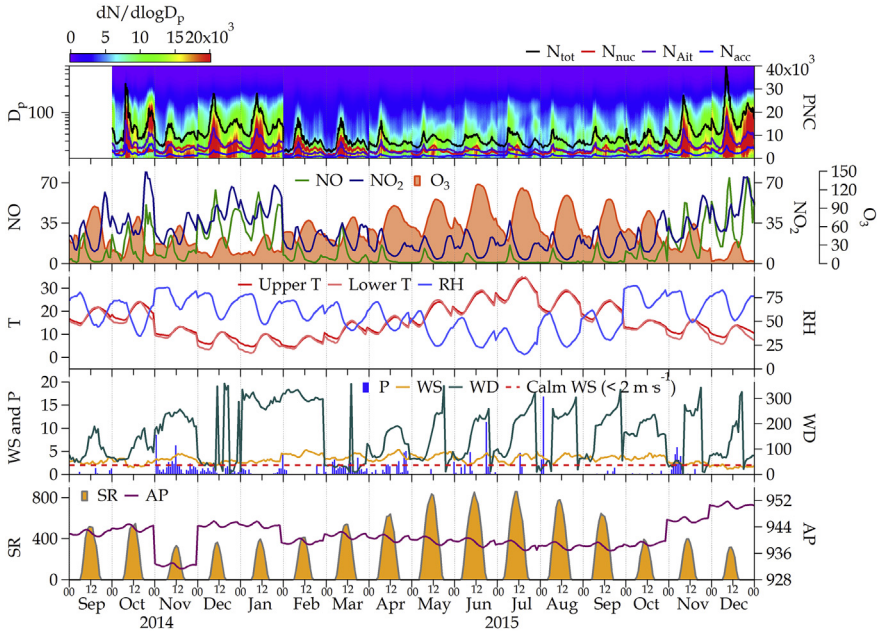

Fig. 2. Monthly daily evolution of the particle number size distributions, gases and meteorological parameters over the whole observation period. Parameters (units) are denoted in the graphs as follows: D_p = particle diameter (nm), PNC = Particle Number Concentration (cm^{-3}); N_{tot} corresponding to Particle Number Total Concentration, N_{nuc} to Nucleation-mode particles, N_{Ait} to Aitken-mode particles and N_{acc} to Accumulation-mode particles, trace gas pollutants (NO, NO_2 and O_3, all in $\mu g\ m^{-3}$), T = Temperature (ºC), RH = Relative Humidity (%), WS = Wind Speed ($m\ s^{-1}$), WD = Wind Direction (degrees), P = Precipitation (mm), SR = Solar Radiation ($W\ m^{-2}$) and AP = Atmospheric Pressure (mbar).

being within the hygroscopic values found for the biogenic aerosol (Shingler et al., 2016). This is in accordance with the main type of GF-PDFs observed in this period, type 2, to which ~60% of the measurements correspond (Fig. S2). At this site, these particles probably originate from NPF bursts (Gómez-Moreno et al., 2011), and the slight increase in their hygroscopicity was related to their aging state (Mochida et al., 2008). The relationship of the hygroscopicity of the newly formed particles in relation to their composition will be examined in a future publication. However, a strong variability in GF_{mean}, as shown by the long whisker at the top of the box (Fig. 3B), was found for cold seasons, especially in large particle sizes. Nitrate ammonium formation from NO_x road traffic emissions (NO_2 in cold seasons was almost three times greater than in warm seasons, Table S3) during severe stagnation episodes (Becerril-Valle, 2018; Plaza et al., 2011), combined with periods without stagnation, was probably responsible of this finding. The influence of sulphate formed in the study area on the hygroscopic properties of aerosol particles is scarce. The dramatic decrease in SO_2 emissions (e.g. SO_2 concentration was $3.1 \pm 2\ \mu g\ m^{-3}$ in winter 2014–2015 and $2.2 \pm 0.5\ \mu g\ m^{-3}$ in spring 2015, Table S3) after the entry into force of European Directive (2003)/17/EC, limiting sulphur in fuels for road traffic, has inhibited sulphate aerosol formation in Madrid (Revuelta et al., 2011). For all sizes NF_{MH} increased in the warm seasons and it was always greater for larger particle sizes, while GF_{MH} decreased (Fig. 3C and D). These findings can be related to the possible contribution of biogenic sources to aerosol particle formation as suggested by the high number of measurements of type 2 and 3 registered during warm months (Fig. S2).

Polar plots of the seasonal variation of GF_{mean}, GF_{MH} and NF_{MH} for different size particles are shown in Fig. S4, S5 and S6. In general, the lowest GF_{mean} values were observed from the northeast to southwest directions where the urban agglomerations are found in the region (Fig. S4). Differently, the highest GF_{mean} were observed from western areas distant away from the direct emission sources (Fig. S4) and, thus, with air masses with significant contributions of background aerosol particles. During the warm seasons NF_{MH} was high for all dry particles (around or greater than 0.50) (Fig. S6), especially for 50 and 80 nm that presented a GF_{MH} ~1.35 (Fig. S5).

Given that H-TDMA data were available for autumns of 2014 and 2015, a comparison between both was possible. As indicated in section 4.1, stagnation episodes were more frequent in autumn 2015 in comparison with autumn 2014, and, thus, the concentrations of aerosol particles, BC (Becerril-Valle et al., 2017) and gases were also higher. Consequently, autumn 2015 registered a remarkable reduction in GF_{mean}, probably related with high BC concentration, as well as in

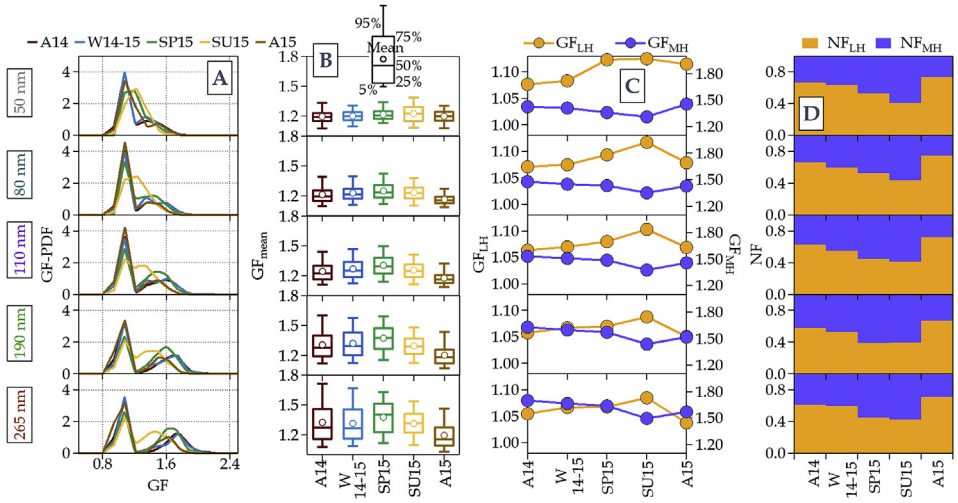

Fig. 3. (A) Seasonal mean GF-PDFs, (B) seasonal whisker and box plot of GF_{mean}, and (C) the GF and (D) the NF for the less (LH) and more hygroscopic (MH) particle group for the different dry particle sizes measured over the whole observation period. The seasons are denoted in the graphs as follows: autumn 2014 = A14, winter 2014–2015 = W14-15, spring 2015 = SP15, summer 2015 = SU15 and autumn 2015 = A15.

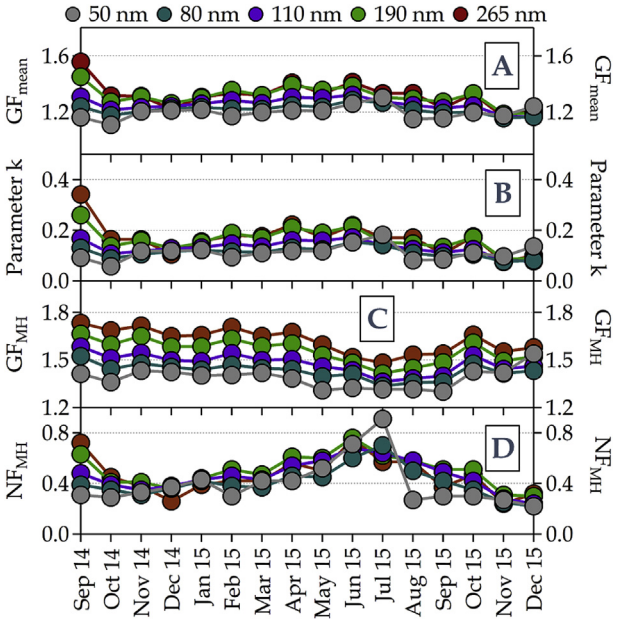

Fig. 4. Monthly mean of (A) GF_{mean}, (B) single hygroscopicity parameter κ, (C) GF_{MH} and (D) NF_{MH} for the different dry particle sizes measured during the whole observation period based on 1-h data.

NF_{MH} and GF_{MH} in all sizes. This result highlights the strong influence of traffic emissions and meteorology on the hygroscopic properties of the aerosol particles.

Monthly distributions of the GF-PDFs for the whole period of measurements are shown in Fig. S7. While GF-PDFs exhibited bimodal distribution in cold months for all sizes, unimodal distributions were observed frequently in warm months for 50 and 80 nm, between May and September 2015. The seasonal variations in the aerosol particle hygroscopicity were also evidenced by a monthly analysis (Fig. 4). GF_{mean} values were higher for the warm months due to an increase in the NF_{MH}, despite GF_{MH} was lower. Aging of SOA species probably produced highly oxidised species and, thus increased the aerosol particle hygroscopicity (Duplissy et al., 2011). GF_{mean} values are well-represented by the hygroscopicity parameter κ, given that both parameters showed a similar behaviour during the study period. This means the difference in GF_{mean} among particle sizes cannot be attributed to Kelvin effect. Thus, it suggests that the hygroscopicity by particle size depended highly on the chemical composition. In warm months κ was the highest, like GF_{mean}, varying from 0.08 to 0.18 for 50, 80 and 110 and varying from 0.15 to 0.22 for 190 and 265 nm (Table S4). Here, it is also worth noting the monthly variations of hygroscopicity observed for 50 nm. The highest GF_{mean} value on average (1.30) was reached in July (36% data coverage (Fig. S1)). At this site, July is one of the months of the warm season that a greater number of NPF bursts occurs (Alonso-Blanco et al., 2017b; Gómez-Moreno et al., 2011). Size-resolved hygroscopicity below a particle diameter of 50 nm will be addressed in a future experimental field campaign at this site.

Aerosol particle hygroscopicity showed size dependence for all months, increasing with particle size. Thus, Aitken mode particles (D_{dry} < 100 nm, i.e. 50, 80 and 110 nm) presented a GF_{mean} between 1.11 and 1.31, while accumulation mode particles (D_{dry} > 100 nm, i.e. 190 and 265 nm) presented higher values, between 1.16 and 1.56 (Table S5A). The variations observed in water uptake by larger and small particles are possibly due to the differences in the chemical composition. In this experimental site, this feature was attributed to the increase in a more hygroscopic coating formed mainly by nitrates and a wide range of aged organic compounds with the increase in particle size. Other authors like Sjogren et al. (2008), Ye et al. (2013) or Jurányi et al. (2013) have reported similar findings in urban and suburban areas, but this has also been observed in other types of areas (Swietlicki et al., 2008).

Hygroscopicities derived from hygroscopic growth data suggested that 50 and 80 nm aerosol particles and 190 and 265 nm aerosol particles exhibited very similar values throughout the study period. Thus, these particle sizes could have a similar chemical composition. These particle sizes only showed a marked difference in hygroscopicity in September 2014 associated with the impact of Bárðarbunga volcanic ash plume on the Iberian Peninsula (Alonso-Blanco et al., 2017c). This episode, together with other events of high hygroscopicity in Madrid, will be studied in a future work.

4.3. Diurnal variation of the aerosol particle hygroscopicity and local sources influence

The typical daily evolution of GF-PDF and GF_{mean} for each season is plotted in Fig. 5. The GF_{mean} exhibited a marked daily variability, which seemed to be driven by the fresh emissions from road traffic in cold seasons and NPF bursts in warm seasons.

The highest GF_{mean} was observed at night (00:00–06:00 UTC) and mid-afternoon (09:00–18:00 UTC), when background aerosol particles were abundant and probably aerosol particles were more aged. Oppositely, particles were found to be more hydrophobic (GF_{mean} was

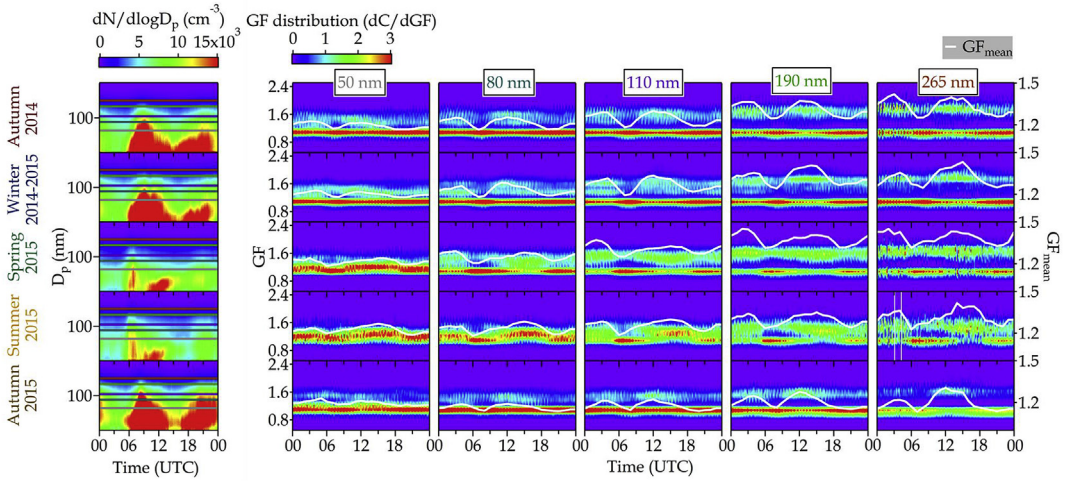

Fig. 5. Contour plots of the seasonal daily mean of the GF-PDFs for the different dry particle sizes measured over the whole observation period, incorporating the seasonal daily mean of the GF_{mean}. Contour plots of the seasonal daily mean of the aerosol particle size distribution have also been incorporated into the graph.

closest to 1.0) during rush-hours; in the morning between 06:00 and 09:00 UTC and at the end of the afternoon, between 18:00 and 22:00 UTC, as other authors have found (Jiang et al., 2016; Kim et al., 2017; Lance et al., 2013), coinciding with the maximum PNC, NO and NO_2 and minimum of O_3 (Fig. 2 and S3). This is explained by the high BC contribution to the content of particles associated with urban traffic emissions reaching the site at that time (Becerril-Valle et al., 2017). In fact, the seasonal variations of the daily H-TDMA data agree with seasonal variations found by Becerril-Valle (2018) for non-refractory compounds obtained from ACSM (ACSM, Aerodyne Research Inc.) measurements during 2014 and from BC measurements during 2015 at the same site. In addition, in autumn 2015, the meteorology and road traffic emissions influence on the daily aerosol particle hygroscopicity are also evidenced (Fig. 5) as was shown in section 4.2. In the warm seasons, the progressive increase in GF_{mean} from the morning rush hour to the afternoon rush hour was especially significant for 50 nm, observing values of ~1.18 and ~1.27 respectively in the rush hour times. As other studies have suggested (Lance et al., 2013; Wu et al., 2016) this increase in the hygroscopicity seemed be related to photo-oxidation of constituents of particles newly formed.

The daily evolution of the type of GF-PDF during all seasons is shown in Fig. 6. While during the cold seasons GF-PDFs were predominantly of type 1 (with two hygroscopic groups) for all sizes, during the warm seasons most GF-PDFs were of type 2 and 3 (with only a hygroscopic group) for 50 and 80 nm. In fact, for these particle sizes it is especially significant during summer the increase of the number of GF-PDF of type 2 (hygroscopic particles) at the expense of a decrease of the type 3 (non-hygroscopic particles) from the midday (when NPF bursts started) to the end of the daylight period. This is possibly associated with the aging of newly formed particles, being this result consistent with those discussed above.

The contribution of urban traffic to the aerosol particle growth factor has been assessed here by a contrast analysis between weekdays (Monday-Friday, WK) and weekend (Saturday-Sunday, WE). Descriptive statistics for the hygroscopic parameters divided into WKs and WEs are presented in Table S6. Aerosol particles during WKs have a slightly lower GF_{mean} (Fig. S8) value and a lower NF_{MH} than that on WEs. This is due to the fact that during WKs traffic emissions were much higher than in WEs as seen in Fig. S9. Thus, the concentrations of SO_2, NO and NO_2 on WEs were lower than on WKs, especially during rush hour times in the morning and afternoon. Oppositely, the O_3 concentration was increased on WEs due to the reduction of NO_x emissions. In warm seasons, SO_2 and NO_x decreased with the reduction in traffic emissions and the enhanced dispersive atmospheric conditions. This was also found in this site by Alonso-Blanco et al. (2018). Therefore, aerosol particles during WEs had a higher hygroscopicity than during WKs. This result is consistent with findings from Enroth et al. (2018) and Massling et al. (2005) in an urban site in Budapest and in an urban background site in Leipzig respectively. These variations are especially significant in summer and autumn 2015, founding the lowest WKs/WEs values for GF_{mean} (0.96–0.97), and NF_{MH} (0.81–0.91) of the study period (Table S6). This can be associated with a significant reduction in traffic during WEs and the effect of meteorology on its emissions. GF_{MH} seemed to be the same or slightly higher in WKs than WEs. Aitken and accumulation mode particles (aged aerosol) are slightly lower during WEs at this site (Alonso-Blanco et al., 2018). Thus, probably the incorporation of aged aerosol particles from traffic emissions into the more hygroscopic particle group could be contributed to a slight increase on the GF_{MH} in WKs.

4.4. Comparison with urban and other suburban sites

The published investigations on hygroscopicity observations of atmospheric aerosol particles obtained by H-TDMA systems in urban areas, both in urban and suburban sites, in the past few years are not many. Only 23 studies were found in the literature (Table S7), of which 7 provided H-TDMA data from suburban sites. With respect to these last ones, Massling et al. (2005) offers the most extensive study to date, analyzing 8-month data in two different periods. A comparison between the results found here and in other sites is presented below, focusing on the differences between urban and suburban sites.

A great variability was found in particles hygroscopic growth among the different locations, study period and dry particle sizes measured, being strongly related to the sources and meteorology. Particle hygroscopicity mostly exhibited multimodal patterns (Table S7), mainly two hygroscopic groups of particles, both in urban and suburban sites. Only one of the hygroscopic groups could be observed in some sites, especially for the smallest sizes measured. This type of structures was associated with fresh combustion particles (Levy et al., 2014) or aging of particles with the same origin (Müller et al., 2017; Wang et al., 2018) or NPF bursts (Gasparini et al., 2004; Kim et al., 2017; Lance et al., 2013; Wu et al., 2016; Zhang et al., 2011) as in CIEMAT site.

Overall, Asian cities are characterized by high population densities and strong industrialization, resulting in high levels of pollution both primary particles and aerosol precursors. This suggests that the hydrophilic aerosol fraction in aerosol particles measured in urban and suburban sites, as it is inferred from NF_{MH} values (Table S7), was higher than for both types of sites in European cities. In general, the highest hygroscopicity values were found in periods of high pollution; in summer for the Asian continent and winter for the European continent.

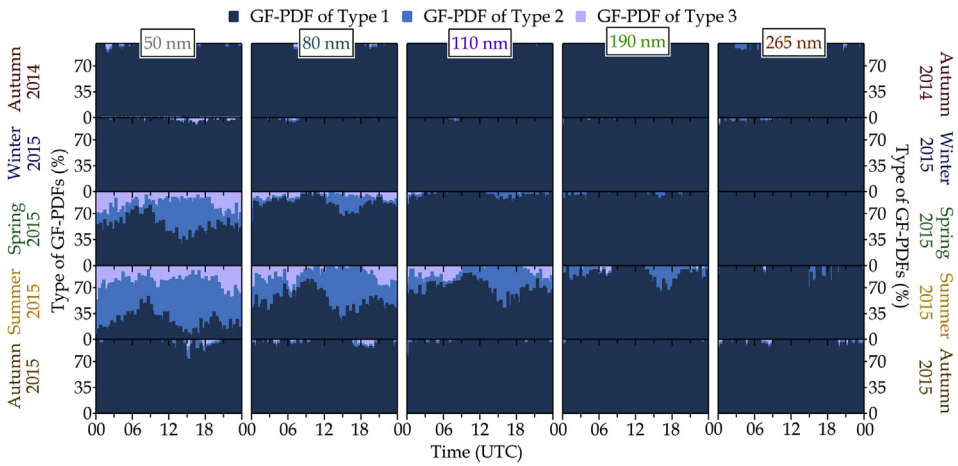

Fig. 6. Seasonal daily evolution of the type of growth factor probability density functions (GF-PDFs) considered in this study: type 1 (externally mixed aerosol particles), type 2 (internally mixed and hygroscopic aerosol particles) and type 3 (internally mixed and non-hygroscopic aerosol particles).

However, although in Madrid the GF_{mean} peaks were identified in winter associated with episodes of high pollution, GF_{mean} on average was higher in summer due to photochemical aging of the particles. This is consistent with the findings of Wu et al. (2016), Ye et al. (2011) and Gasparini et al. (2004), who observed an increase in aerosol particle hygroscopicity during NPF bursts related to photo-oxidation of organics constituents and an increase of soluble material (inorganics).

As discussed in section 4.2, the atmospheric lifetime of aerosol has an important influence on aerosol particle hygroscopicity. So, and except for Yeung et al. (2014) and Ye et al. (2013), all the authors agree that aerosol hygroscopicity increases when dry particle size increases which is related to their aging or hydrophilic coating. In this respect, clear changes in the hygroscopicity of the smallest particles are linked with their subsequent aging, as were reported in other studies (Gasparini et al., 2004; Ye et al., 2013) and as it has been found in this work. Thus, it is interesting to compare our results with those obtained in urban and other suburban sites. This has been done based on two aerosol particle sizes; 50 (representing the fresh aerosol) and 265 (representing the aged aerosol) nm or similar particle sizes (Table S7).

Hygroscopic growth factor from the current study seems to be similar to those found in suburban European locations and lower than those obtained in suburban Asian sites, in the same way that the NF_{MH}. GF_{mean} for 50 nm in Madrid are similar to the average of a suburban Paris site (Laborde et al., 2013), ~1.20, and slightly higher than in urban sites of Munich (Ferron et al., 2005) or Budapest (Enroth et al., 2018). However, GF_{mean} and NF_{MH} in Madrid for the same dry particle size (50 nm) were 1–2 times lowers than that of suburban Asian sites (Table S7). In the case of larger particles, ~265 nm, these differences were similar to those found for 50 nm. Regarding urban sites, Madrid presented GF_{mean} and NF_{MH} values relatively higher than urban European sites, but lower than urban Asian sites. Given the limited information on aerosol hygroscopicity in the American continent (Table S7) it is not possible to make comparisons to the results obtained in this study. Although this section is focused on aerosol particle hygroscopicity differences between urban and suburban sites, other types of measurement sites are also discussed here for their comparison. The aerosol hygroscopic growth characteristics in suburban sites contrast with those for other types of sites such as high-altitude (Holmgren et al., 2014; Kammermann et al., 2010), rural (Adam et al., 2012; Fors et al., 2011; Mamali et al., 2018) or coastal (Gysel et al., 2007; Park et al., 2009). In these sites, two hygroscopic groups of particles were also commonly observed, however there is a wide range of results. For example, in high-altitude sites the aerosol particle hygroscopicity seems to be influenced by the injection of pollutants from the boundary layer. Thus, CIEMAT site values were found more similar to Puy de Dôme site (1465 m a.s.l) (Holmgren et al., 2014) than to Jungfraujoch site (3580 m a.s.l.) (Kammermann et al., 2010). GF were slightly higher in rural sites than at CIEMAT, possibly as a result of a low impact of anthropogenic local sources of aerosol particles and a further aerosol particle aging. In Fors et al. (2011) GF_{mean} varied from 1.27 (35 nm) to 1.58 (265 nm) and in Adam et al. (2012) GF_{mean} varied from 1.10 (35 nm) to 1.48 (265 nm). Coastal sites registered even higher values (GF above 2.0) than suburban sites associated with marine aerosol (Swietlicki et al. (2008) and references therein). In all these sites, as in CIEMAT suburban site, size dependence of particle hygroscopicity was also found, the larger particles the greater the hygroscopicity.

This section highlights the lack of knowledge that exists regarding size-resolved hygroscopic properties of submicron particles, especially in suburban sites. In addition, from this comparison it follows that meteorology and sources information, as well as aerosol particles composition, are needed to explain the different hygroscopic behavior in each specific measurement site.

5. Conclusions

The results obtained of the size-resolved hygroscopicity of submicrometer aerosol particles in a suburban area of the Southern Europe are presented in this work. 16-months of H-TDMA measurements for size particles of 50, 80, 110, 190 and 265 nm have been analysed in this study.

Mixing state of aerosol particles was significantly different among seasons. Aerosols were often externally mixed, exhibiting two different hygroscopic groups. Particles were more externally mixed in cold seasons than in warm ones, being driven by pollution accumulating and nitrate formation. Therefore, GF_{MH} reached the highest seasonal values (1.46 for 50 nm-1.70 for 265 nm) while the NF_{MH} was reduced (< 0.50). Oppositely, atmospheric dispersive conditions and a meteorology enhancing NPF bursts in warm seasons implied that the aerosol particles were often internally mixed. GF_{mean} was higher during warm than cold seasons, e.g. 1.23 vs 1.20 for 50 nm or 1.38 vs 1.19 for 265 nm, due to a higher aerosol particle aging, both from recently formed and background particles. Generally, in all seasons the particle hygroscopicity tended to increase with size, probably because of a more hygroscopic coating by chemical aging and an increase of inorganic species.

Diurnal cycle in particle hygroscopicity was strongly dependent on the aerosol origin (traffic influence), especially in cold seasons. Particle hygroscopicity exhibited a good anticorrelation with the traffic emission pattern, founding the minimum GF_{mean} values during rush hours. The WKs/WEs ratio for GF_{mean} and NF_{MH} were < 1.00, with values close to or slightly greater than 1.00 for GF_{MH} during all seasons. The reduction of traffic emissions during WEs led to background particles (aged aerosol) probably contributed to the greater hygroscopicity on average than that found in WKs.

Our results pointed out that aerosol particle hygroscopicity in CIEMAT suburban site was similar to those found in other suburban European sites and relatively lower than in urban European ones. However, hygroscopicity values in CIEMAT were lower than in suburban and urban Asian sites. Despite the gaps in present knowledge on aerosol particles hygroscopicity in suburban sites in the literature, this comparison highlights the importance of sources, and thus aerosol composition, and meteorology on aerosol particles hygroscopicity. The wide variety of emission sources makes the properties of the fresh aerosols be very diverse. The continuous changes that they suffer in the atmosphere throughout the different processes during their lifetime may increase the aerosol particle hygroscopicity which can involve immediate changes in the particle size. As this work shows, studies addressing this property are still scarce, although they can provide important inputs for modelling the aerosol particle hygroscopic behavior in the atmosphere at different spatial scales and predict the aerosol particle size variation with humidity. Thus, these results not only contribute to further understanding the hygroscopic behavior of suburban aerosol particles, but they can also be used for parameterizing and validating aerosol particle behavior in atmospheric and climate models.

Acknowledgements

This work has been supported by the Ministry of Science, Innovation and Universities through the project CRISOL (CGL2017-85344-R) funded by AEI/FEDER, UE, by the Autonomous Community of Madrid through the projects AIRTEC (P2018/EMT-4329) and TIGAS-CM (Y2018/EMT-5177) and by Red de Excelencia ACTRIS-ESPAÑA (CGL2017-90884-REDT). The authors are grateful to Martin Gysel for the development of $TDMA_{fit}$ algorithm to invert H-TDMA raw data ($TDMA_{inv}$) and allowing free use within the scientific community. We also thank to Diego Alberto Alonso, José Luis Mosquera and Francisco Molero for their help in the development of the analysis procedures for processing H-TDMA data, especially to Diego Alberto for his help in the hygroscopic groups-fitting procedure development from the MATLAB program.

Appendix A. Supplementary data

Supplementary data to this article can be found online at https://doi.org/10.1016/j.atmosenv.2019.05.065.

References

Adam, M., Putaud, J., Martins dos Santos, S., Dell'Acqua, A., Gruening, C., 2012. Aerosol hygroscopicity at a regional background site (Ispra) in Northern Italy. Atmos. Chem. Phys. 12, 5703–5717.

Alonso-Blanco, E., Gómez-Moreno, F., Artíñano, B., Iglesias-Samitier, S., Juncal-Bello, V., Piñeiro-Iglesias, M., López-Mahía, P., Pérez, N., Brines, M., Alastuey, A., 2018. Temporal and spatial variability of atmospheric particle number size distributions across Spain. Atmos. Environ. 190, 146–160.

Alonso-Blanco, E., Gómez-Moreno, F., Coz, E., Díaz, E., Peréz, N., Alastuey, A., Querol, X., Reche, C., Titos, G., Ealo, M., Tritscher, T., Filimundi, E., Latorre, E., Artiñano, B., 2017a. Hygroscopic Properties of Freshly Formed Particles during an Intensive Summertime Field Campaign in Madrid. 5th Iberian Meeting on Aerosol Science and Technology, Barcelona (Spain) Abstract Book-RICTA2017, 4-6 Jul 2017.

Alonso-Blanco, E., Gómez-Moreno, F., Núñez, L., Pujadas, M., Cusack, M., Artíñano, B., 2017b. Aerosol particle shrinkage event phenomenology in a South European suburban area during 2009–2015. Atmos. Environ. 160, 154–164.

Alonso-Blanco, E., Gómez-Moreno, F.J., Becerril-Valle, M., Coz, E., Díaz, E., Artíñano, B., 2017c. Hygroscopic Properties of Different Aerosol Types at a Suburban Site (Madrid) in the Iberian Peninsula, European Aerosol Conference (EAC). Abstracts Book, Zurich (Switzerland).

Alonso-Blanco, E., Gómez-Moreno, F.J., Sjögren, S., Artíñano, B., 2014. Building, tune-up and first measurements of aerosol hygroscopicity with an HTDMA. In: 2nd Iberian Meeting on Aerosol Science and Technology. Publicacions Universitat Rovira i Virgili, Tarragona, Spain, pp. 187 28-30 June.

Artíñano, B., Salvador, P., Alonso, D.G., Querol, X., Alastuey, A., 2003. Anthropogenic and natural influence on the PM10 and PM2. 5 aerosol in Madrid (Spain). Analysis of high concentration episodes. Environ. Pollut. 125, 453–465.

Becerril-Valle, M., 2018. Physico-chemical Properties of the Atmospheric Aerosols in Urban and Rural Areas in Southern Europe. Ph.D. Thesis. Universidad Complutense de Madrid, Spain.

Becerril-Valle, M., Coz, E., Prévôt, A., Močnik, G., Pandis, S., de la Campa, A.S., Alastuey, A., Díaz, E., Pérez, R., Artíñano, B., 2017. Characterization of atmospheric black carbon and co-pollutants in urban and rural areas of Spain. Atmos. Environ. 169, 36–53.

Boreddy, S., Kawamura, K., Bikkina, S., Sarin, M., 2016. Hygroscopic growth of particles nebulized from water-soluble extracts of PM2. 5 aerosols over the Bay of Bengal: influence of heterogeneity in air masses and formation pathways. Sci. Total Environ. 544, 661–669.

Boreddy, S., Kawamura, K., Jung, J., 2014a. Hygroscopic properties of particles nebulized from water extracts of aerosols collected at Chichijima Island in the western North Pacific: an outflow region of Asian dust. J. Geophys. Res.: Atmospheres 119, 167–178.

Boreddy, S., Kawamura, K., Mkoma, S., Fu, P., 2014b. Hygroscopic behavior of water-soluble matter extracted from biomass burning aerosols collected at a rural site in Tanzania, East Africa. J. Geophys. Res.: Atmos 119 (12) 233-212,245.

Crespí, S.N., Artíñano, B., Cabal, H., 1995. Synoptic classification of the mixed-layer height evolution. J. Appl. Meteorol. 34, 1666–1677.

Chen, L.-Y., Jeng, F.-T., Chen, C.-C., Hsiao, T.-C., 2003. Hygroscopic behavior of atmospheric aerosol in Taipei. Atmos. Environ. 37, 2069–2075.

Cheung, H.H., Yeung, M.C., Li, Y.J., Lee, B.P., Chan, C.K., 2015. Relative humidity-dependent HTDMA measurements of ambient aerosols at the HKUST supersite in Hong Kong, China. Aerosol Sci. Technol. 49, 643–654.

Davis, E.J., Buehler, M.F., Ward, T.L., 1990. The double-ring electrodynamic balance for microparticle characterization. Rev. Sci. Instrum. 61, 1281–1288.

Duplissy, J., DeCarlo, P., Dommen, J., Alfarra, M., Metzger, A., Barmpadimos, I., Prevot, A., Weingartner, E., Tritscher, T., Gysel, M., 2011. Relating hygroscopicity and composition of organic aerosol particulate matter. Atmos. Chem. Phys. 11, 1155–1165.

Duplissy, J., Gysel, M., Sjogren, S., Meyer, N., Good, N., Kammermann, L., Michaud, V., Weigel, R., Gruening, S., Martins dos Santos, C., 2009. Intercomparison study of six HTDMAs: results and recommendations. Atmos. Measure. Techniques 2, 363–378.

Enroth, J., Mikkilä, J., Németh, Z., Kulmala, M., Salma, I., 2018. Wintertime hygroscopicity and volatility of ambient urban aerosol particles. Atmos. Chem. Phys. 18, 4533–4548.

Ferron, G., Karg, E., Busch, B., Heyder, J., 2005. Ambient particles at an urban, semi-urban and rural site in Central Europe: hygroscopic properties. Atmos. Environ. 39, 343–352.

Fors, E.O., Swietlicki, E., Svenningsson, B., Kristensson, A., Frank, G.P., Sporre, M., 2011. Hygroscopic properties of the ambient aerosol in southern Sweden–a two year study. Atmos. Chem. Phys. 11, 8343–8361.

Gasparini, R., Li, R., Collins, D.R., 2004. Integration of size distributions and size-resolved hygroscopicity measured during the Houston Supersite for compositional categorization of the aerosol. Atmos. Environ. 38, 3285–3303.

Gómez-Moreno, F., Pujadas, M., Plaza, J., Rodríguez-Maroto, J., Martínez-Lozano, P., Artíñano, B., 2011. Influence of seasonal factors on the atmospheric particle number concentration and size distribution in Madrid. Atmos. Environ. 45, 3169–3180.

Gómez-Moreno, F.J., Alonso, E., Artíñano, B., Juncal-Bello, V., Iglesias-Samitier, S., Piñeiro Iglesias, M., Mahía, P.L., Pérez, N., Pey, J., Ripoll, A., 2015. Intercomparisons of mobility size spectrometers and condensation particle counters in the frame of the Spanish atmospheric observational aerosol network. Aerosol Sci. Technol. 49, 777–785.

Gysel, M., Crosier, J., Topping, D., Whitehead, J., Bower, K., Cubison, M., Williams, P., Flynn, M., McFiggans, G., Coe, H., 2007. Closure study between chemical composition and hygroscopic growth of aerosol particles during TORCH2. Atmos. Chem. Phys. 7, 6131–6144.

Gysel, M., McFiggans, G., Coe, H., 2009. Inversion of tandem differential mobility analyser (TDMA) measurements. J. Aerosol Sci. 40, 134–151.

Holmgren, H., Sellegri, K., Hervo, M., Rose, C., Freney, E., Villani, P., Laj, P., 2014. Hygroscopic properties and mixing state of aerosol measured at the high-altitude site Puy de Dôme (1465 m asl), France. Atmos. Chem. Phys. 14, 9537–9554.

IPCC, 2001. IPCC 2001: Climate Change 2001. The Climate Change Contribution of Working Group I to the Third Assessment Report of the Intergovemmental Panel on Climate Change 159.

Jiang, R., Tan, H., Tang, L., Cai, M., Yin, Y., Li, F., Liu, L., Xu, H., Chan, P., Deng, X., 2016. Comparison of aerosol hygroscopicity and mixing state between winter and summer seasons in Pearl River Delta region, China. Atmos. Res. 169, 160–170.

Jimenez, J.L., Canagaratna, M., Donahue, N., Prevot, A., Zhang, Q., Kroll, J.H., DeCarlo, P.F., Allan, J.D., Coe, H., Ng, N., 2009. Evolution of organic aerosols in the atmosphere. Science 326, 1525–1529.

Jurányi, Z., Tritscher, T., Gysel, M., Laborde, M., Gomes, L., Roberts, G., Baltensperger, U., Weingartner, E., 2013. Hygroscopic mixing state of urban aerosol derived from size-resolved cloud condensation nuclei measurements during the MEGAPOLI campaign in Paris. Atmos. Chem. Phys. 13, 6431–6446.

Kamilli, K., Poulain, L., Held, A., Nowak, A., Birmili, W., Wiedensohler, A., 2014. Hygroscopic properties of the Paris urban aerosol in relation to its chemical composition. Atmos. Chem. Phys. 14, 737–749.

Kammermann, L., Gysel, M., Weingartner, E., Baltensperger, U., 2010. 13-month climatology of the aerosol hygroscopicity at the free tropospheric site Jungfraujoch (3580 m asl). Atmos. Chem. Phys. 10, 10717–10732.

Kim, N., Park, M., Yum, S.S., Park, J.S., Song, I.H., Shin, H.J., Ahn, J.Y., Kwak, K.-H., Kim, H., Bae, G.-N., 2017. Hygroscopic properties of urban aerosols and their cloud condensation nuclei activities measured in Seoul during the MAPS-Seoul campaign. Atmos. Environ. 153, 217–232.

Kulkarni, P., Baron, P.A., Willeke, K., 2011. Aerosol Measurement: Principles, Techniques, and Applications. John Wiley & Sons.

Laborde, M., Crippa, M., Tritscher, T., Jurányi, Z., Decarlo, P., Temime-Roussel, B., Marchand, N., Eckhardt, S., Stohl, A., Baltensperger, U., 2013. Black carbon physical properties and mixing state in the European megacity Paris. Atmos. Chem. Phys. 13, 5831–5856.

Lance, S., Raatikainen, T., Onasch, T.B., Worsnop, D.R., Yu, X.-Y., Alexander, M., Stolzenburg, M., McMurry, P., Smith, J.N., Nenes, A., 2013. Aerosol mixing state, hygroscopic growth and cloud activation efficiency during MIRAGE 2006. Atmos. Chem. Phys. 13, 5049–5062.

Levy, M.E., Zhang, R., Zheng, J., Tan, H., Wang, Y., Molina, L.T., Takahama, S., Russell, L., Li, G., 2014. Measurements of submicron aerosols at the California–Mexico border during the Cal–Mex 2010 field campaign. Atmos. Environ. 88, 308–319.

Liu, B., Pui, D., Whitby, K., Kittelson, D., Kousaka, Y., McKenzie, R., 1978. The aerosol mobility chromatograph: a new detector for sulfuric acid aerosols. Atmos. Environ. 12, 99–104 1967.

Liu, D., Allan, J., Whitehead, J., Young, D., Flynn, M., Coe, H., McFiggans, G., Fleming, Z.L., Bandy, B., 2013. Ambient black carbon particle hygroscopic properties controlled by mixing state and composition. Atmos. Chem. Phys. 13, 2015–2029.

Mamali, D., Mikkilä, J., Henzing, B., Spoor, R., Ehn, M., Petäjä, T., Russchenberg, H., Biskos, G., 2018. Long-term observations of the background aerosol at Cabauw, The Netherlands. Sci. Total Environ. 625, 752–761.

Massling, A., Stock, M., Wiedensohler, A., 2005. Diurnal, weekly, and seasonal variation of hygroscopic properties of submicrometer urban aerosol particles. Atmos. Environ. 39, 3911–3922.

Mochida, M., Miyakawa, T., Takegawa, N., Morino, Y., Kawamura, K., Kondo, Y., 2008. Significant alteration in the hygroscopic properties of urban aerosol particles by the secondary formation of organics. Geophys. Res. Lett. 35.

Müller, A., Miyazaki, Y., Aggarwal, S.G., Kitamori, Y., Boreddy, S.K., Kawamura, K., 2017. Effects of chemical composition and mixing state on size-resolved hygroscopicity and cloud condensation nuclei activity of submicron aerosols at a suburban site in northern Japan in summer. J. Geophys. Res.: Atmospheres 122, 9301–9318.

Nilsson, E., Swietlicki, E., Sjogren, S., Löndahl, J., Nyman, M., Svenningsson, B., 2009. Development of an H-TDMA for long-term unattended measurement of the hygroscopic properties of atmospheric aerosol particles. Atmos. Measure. Techniques 2, 313–318.

Park, K., Kim, J.-S., Park, S.H., 2009. Measurements of hygroscopicity and volatility of atmospheric ultrafine particles during ultrafine particle formation events at urban, industrial, and coastal sites. Environ. Sci. Technol. 43, 6710–6716.

Petters, M., Kreidenweis, S., 2007. A single parameter representation of hygroscopic growth and cloud condensation nucleus activity. Atmos. Chem. Phys. 7, 1961–1971.

Plaza, J., Pujadas, M., Gómez-Moreno, F., Sánchez, M., Artíñano, B., 2011. Mass size distributions of soluble sulfate, nitrate and ammonium in the Madrid urban aerosol. Atmos. Environ. 45, 4966–4976.

Pöschl, U., 2005. Atmospheric aerosols: composition, transformation, climate and health effects. Angew. Chem. Int. Ed. 44, 7520–7540.

Raoult, F.-M., 1887. Loi générale des tensions de vapeur des dissolvants. C. R. Hebd. Seances Acad. Sci. 104, 1430–1433.

Revuelta, M.A., Gómez-Moreno, F.J., Núñez, L., Artíñano, B., Palacios, M., 2011. Analysis of a Time Series of Particulate Sulfate in a Suburban Site: Time Evolution and Characterization of Events, European Aerosol Conference-EAC 2011. Abstracts Book,

Manchester (England).
Rood, M.J., Larson, T.V., Covert, D.S., Ahlquist, N.C., 1985. Measurement of laboratory and ambient aerosols with temperature and humidity controlled nephelometry. Atmos. Environ. 19, 1181–1190 1967.
Saiz-Lopez, A., Borge, R., Notario, A., Adame, J.A., De la Paz, D., Querol, X., Artíñano, B., Gómez-Moreno, F.J., Cuevas, C.A., 2017. Unexpected increase in the oxidation capacity of the urban atmosphere of Madrid, Spain. Sci. Rep. 7, 45956.
Shingler, T., Crosbie, E., Ortega, A., Shiraiwa, M., Zuend, A., Beyersdorf, A., Ziemba, L., Anderson, B., Thornhill, L., Perring, A.E., 2016. Airborne characterization of subsaturated aerosol hygroscopicity and dry refractive index from the surface to 6.5 km during the SEAC4RS campaign. J. Geophys. Res.: Atmospheres 121, 4188–4210.
Sjogren, S., Gysel, M., Weingartner, E., Alfarra, M., Duplissy, J., Cozic, J., Crosier, J., Coe, H., Baltensperger, U., 2008. Hygroscopicity of the submicrometer aerosol at the high-alpine site Jungfraujoch, 3580 m asl, Switzerland. Atmos. Chem. Phys. 8, 5715–5729.
Solomon, S., Qin, D., Manning, M., Averyt, K., Marquis, M., 2007. Climate Change 2007-the Physical Science Basis: Working Group I Contribution to the Fourth Assessment Report of the IPCC. Cambridge university press.
Swietlicki, E., Hansson, H.C., Hämeri, K., Svenningsson, B., Massling, A., McFiggans, G., McMurry, P., Petäjä, T., Tunved, P., Gysel, M., 2008. Hygroscopic properties of submicrometer atmospheric aerosol particles measured with H-TDMA instruments in various environments-A review. Tellus B 60, 432–469.
Thomson, W., 1872. 4. On the equilibrium of vapour at a curved surface of liquid. Proc. Royal. Soc. Edinburgh 7, 63–68.
Tritscher, T., Dommen, J., DeCarlo, P., Gysel, M., Barmet, P., Praplan, A., Weingartner, E., Prévôt, A., Riipinen, I., Donahue, N., 2011. Volatility and hygroscopicity of aging secondary organic aerosol in a smog chamber. Atmos. Chem. Phys. 11, 11477–11496.
Wang, Y., Wu, Z., Ma, N., Wu, Y., Zeng, L., Zhao, C., Wiedensohler, A., 2018. Statistical analysis and parameterization of the hygroscopic growth of the sub-micrometer urban background aerosol in Beijing. Atmos. Environ. 175, 184–191.
Wiedensohler, A., Birmili, W., Nowak, A., Sonntag, A., Weinhold, K., Merkel, M., Wehner, B., Tuch, T., Pfeifer, S., Fiebig, M., Fjäraa, A.M., Asmi, E., Sellegri, K., Depuy, R., Venzac, H., Villani, P., Laj, P., Aalto, P., Ogren, J.A., Swietlicki, E., Williams, P., Roldin, P., Quincey, P., Hüglin, C., Fierz-Schmidhauser, R., Gysel, M., Weingartner, E., Riccobono, F., Santos, S., Grüning, C., Faloon, K., Beddows, D., Harrison, R., Monahan, C., Jennings, S.G., O'Dowd, C.D., Marinoni, A., Horn, H.-G., Keck, L., Jiang, J., Scheckman, J., McMurry, P.H., Deng, Z., Zhao, C.S., Moerman, M., Henzing, B., de Leeuw, G., Löschau, G., Bastian, S., 2012. Particle mobility size spectrometers: harmonization of technical standards and data structure to facilitate high quality long-term observations of atmospheric particle number size distributions. Atmos. Measure. Techniques 5, 657–685.
Wu, Z., Zheng, J., Shang, D., Du, Z., Wu, Y., Zeng, L., Wiedensohler, A., Hu, M., 2016. Particle hygroscopicity and its link to chemical composition in the urban atmosphere of Beijing, China, during summertime. Atmos. Chem. Phys. 16, 1123–1138.
Ye, X., Ma, Z., Hu, D., Yang, X., Chen, J., 2011. Size-resolved hygroscopicity of submicrometer urban aerosols in Shanghai during wintertime. Atmos. Res. 99, 353–364.
Ye, X., Tang, C., Yin, Z., Chen, J., Ma, Z., Kong, L., Yang, X., Gao, W., Geng, F., 2013. Hygroscopic growth of urban aerosol particles during the 2009 Mirage-Shanghai Campaign. Atmos. Environ. 64, 263–269.
Yeung, M.C., Lee, B.P., Li, Y.J., Chan, C.K., 2014. Simultaneous HTDMA and HR-ToF-AMS measurements at the HKUST supersite in Hong Kong in 2011. J. Geophys. Res.: Atmospheres 119, 9864–9883.
Zhang, J., Wang, L., Chen, J., Feng, S., Shen, J., Jiao, L., 2011. Hygroscopicity of ambient submicron particles in urban Hangzhou, China. Front. Environ. Sci. Eng. China 5, 342.